HOMOTOPY ANALYSIS METHOD FOR MIXED CONVECTIVE BOUNDARY LAYER FLOW OF A NANOFLUID OVER A VERTICAL CIRCULAR CYLINDER

by

Saeed DINARVAND [a*], Abbas ABBASSI [a], Reza HOSSEINI [a], and Ioan POP [b]

[a] Mechanical Engineering Department, Amirkabir University of Technology, Tehran, Iran
[b] Mathematics Department, University of Cluj, Cluj, Romania

Original scientific paper
DOI: 10.2298/TSCI120225165D

This article deals with the study of the steady axisymmetric mixed convective boundary layer flow of a nanofluid over a vertical circular cylinder with prescribed external flow and surface temperature. By means of similarity transformation, the governing partial differential equations are reduced into highly non-linear ordinary differential equations. The resulting non-linear system has been solved analytically using an efficient technique namely homotopy analysis method. Expressions for velocity and temperature fields are developed in series form. In this study, three different types of nanoparticles are considered, namely alumina (Al_2O_3), titania (TiO_2), and copper (Cu) with water as the base fluid. For copper-water nanofluid, graphical results are presented to describe the influence of the nanoparticle volume fraction on the velocity and temperature fields for the forced and mixed convection flows. Moreover, the features of the flow and heat transfer characteristics are analyzed and discussed for foregoing nanofluids. It is found that the skin friction coefficient and the heat transfer rate at the surface are highest for copper-water nanofluid compared to the alumina-water and titania-water nanofluids.

Key words: *mixed convection, vertical circular cylinder, nanofluids, nanoparticle volume fraction, homotopy analysis method*

Introduction

Nanofluids are prepared by dispersing solid nanoparticles in fluids such as water, oil, or ethylene glycol. These fluids represent an innovative way to increase thermal conductivity and, therefore, heat transfer. Unlike heat transfer in conventional fluids, the exceptionally high thermal conductivity of nanofluids provides for enhanced heat transfer rates, a unique feature of nanofluids. Advances in device miniaturization have necessitated heat transfer systems that are small in size, light mass, and high performance.

Mixed convection flows, or combined free and forced convection flows, occur in many technological and industrial applications and in nature. Some examples include solar receivers exposed to wind currents, electronic devices cooled by fans, nuclear reactors cooled during emergency shutdown, heat exchanges placed in a low-velocity environment, flows in the ocean and in the atmosphere, and many more. A comprehensive review of buoyancy induced

* Corresponding author; e-mail: saeed_dinarvand@yahoo.com; dinarvand@aut.ac.ir

flows is given in the monograph by Gebart *et al.* [1], and Martynenko and Khramtsov [2]. The mixed convection boundary layer flow past a vertical cylinder is a classical problem and has been studied by many investigators. Chen and Mucoglu [3] have investigated the effects of mixed convection over a vertical slender cylinder due to the thermal diffusion with prescribed wall temperature and the solution was obtained by using the local non-similarity method. Further, Mahmood and Merkin [4] have solved this problem using an implicit finite difference scheme. Ishak *et al.* [5] analyzed the effects of injection and suction on the steady mixed convection boundary layer flows over a vertical slender cylinder with a free stream velocity and a wall surface temperature proportional to the axial distance along the surface of the cylinder.

Most scientific problems and phenomena are modeled by non-linear ordinary or partial differential equations. As an example, boundary layer flows can be mentioned. Therefore, the study on the various methods used for solving the non-linear differential equations is a very important topic for the analysis of engineering practical problems. There are a number of approaches for solving non-linear equations, which range from completely analytical to completely numerical ones. Besides all advantages of using numerical methods, closed form solutions appear more appealing because they reveal physical insights through the physics of the problem. Also, parametric studies become more convenient with applying analytical methods.

The homotopy analysis method (HAM) [6-13] is a general analytic approach to get series solutions of various types of non-linear equations, including algebraic equations, ordinary differential equations, partial differential equations, differential-integral equations, differential-difference equation, and coupled equations of them. Unlike perturbation methods, the HAM is independent of small/large physical parameters, and thus is valid no matter whether a non-linear problem contains small/large physical parameters or not. More importantly, different from all perturbation and traditional non-perturbation methods, the HAM provides us a simple way to ensure the convergence of solution series, and therefore, the HAM is valid even for strongly non-linear problems. Besides, different from all perturbation and previous non-perturbation methods, the HAM provides us with great freedom to choose proper base functions to approximate a non-linear problem [7, 12]. In recent years, the HAM has been successfully employed to solve many types of non-linear problems such as the non-linear equations arising in heat transfer [14], the non-linear model of diffusion and reaction in porous catalysts [15], the non-homogeneous Blasius problem [16], the generalized 3-D MHD flow over a porous stretching sheet [17], the wire coating analysis using MHD Oldroyd 8-constant fluid [18], the viscous flow over a non-linearly stretching sheet [19], the off-centered stagnation flow towards a rotating disc [20], the nano boundary layer flows [21], the boundary-layer flow about a heated and rotating down-pointing vertical cone [22], the 2-D viscous flow in a rectangular domain bounded by two moving porous walls [23], the unsteady laminar MHD flow near forward stagnation point of an impulsively rotating and translating sphere in presence of buoyancy forces [24], the non-similarity boundary-layer flows over a porous wedge [25], the steady flow and heat transfer of a Sisko fluid in annular pipe [26], the steady flow of an Oldroyd 8-constant fluid due to a suddenly moved plate [27], the MHD flow of non-Newtonian nanofluid and heat transfer in coaxial porous cylinder [28], the non-Newtonian nanofluids with Reynolds' model and Vogel's model [29], and the flow of non-Newtonian nanofluid in a pipe [30]. These new solutions have never been reported by all other previous analytic methods. This shows the great potential of the HAM for strongly non-linear problems in science and engineering.

The main goal of the present study is to find the completely analytical solution for the steady axisymmetric mixed convective boundary layer flow of a nanofluid over a vertical circular cylinder. The model introduced by Tiwari and Das [31] has been used in the present study.

The resulting non-linear system has been solved analytically using an efficient technique namely HAM. Finally, the results are reported for three different types of nanoparticles namely alumina, titania, and copper with water as the base fluid.

Nanofluid flow analysis and mathematical formulation

Let us consider the steady axisymmetric mixed convective boundary layer flow of a nanofluid over a vertical circular cylinder with prescribed external flow and surface temperature. It is assumed that the mainstream velocity is $U(x)$ and the temperature of the ambient nanofluid is T_∞, while the temperature of the cylinder is $T_w(x)$. Under these assumptions and using the model of the nanofluid proposed by Tiwari and Das [31], the boundary layer equations governing the flow can be written as [32]:

$$\frac{\partial}{\partial x}(ru)+\frac{\partial}{\partial r}(rw)=0 \tag{1}$$

$$u\frac{\partial u}{\partial x}+w\frac{\partial u}{\partial r}=U\frac{\mathrm{d}U}{\mathrm{d}x}+\nu_{\mathrm{nf}}\left(\frac{\partial^2 u}{\partial r^2}+\frac{1}{r}\frac{\partial u}{\partial r}\right)+\frac{\varphi\rho_{\mathrm{s}}\beta_{\mathrm{s}}+(1-\varphi)\rho_{\mathrm{f}}\beta_{\mathrm{f}}}{\rho_{\mathrm{nf}}}\mathrm{g}(T-T_\infty) \tag{2}$$

$$u\frac{\partial T}{\partial x}+w\frac{\partial T}{\partial r}=\alpha_{nf}\left(\frac{\partial^2 T}{\partial r^2}+\frac{1}{r}\frac{\partial T}{\partial r}\right) \tag{3}$$

The corresponding boundary conditions are:

$$\begin{aligned} &u=w=0, && T=T_{\mathrm{w}}(x)=T_\infty \Delta T\left(\frac{x}{\ell}\right), && \text{at} \quad r=a,\\ &u=U(x)\to U_\infty\left(\frac{x}{\ell}\right), && T\to T_\infty, && \text{at} \quad r\to\infty \end{aligned} \tag{4}$$

In this equations, x and r are Cartesian co-ordinates measured in the axial and radial directions, respectively, u and w – the velocity components along x and r directions, T is the temperature of the nanofluid, β – the coefficient of thermal expansion, and ρ_{f} and ρ_{s} are the densities of the fluid and of the solid fractions, respectively. Here, ν_{nf} is the kinematic viscosity of the nanofluid and α_{nf} is the thermal diffusivity of the nanofluid, which are given by [33]:

$$\nu_{\mathrm{nf}}=\frac{\mu_{\mathrm{f}}}{(1-\varphi)^{2.5}[(1-\varphi)\rho_{\mathrm{f}}+\varphi\rho_{\mathrm{s}})]} \tag{5}$$

$$\rho_{\mathrm{nf}}=(1-\varphi)\rho_{\mathrm{f}}+\varphi\rho_{\mathrm{s}} \tag{6}$$

$$\alpha_{\mathrm{nf}}=\frac{k_{\mathrm{nf}}}{(\rho C_p)_{\mathrm{nf}}} \tag{7}$$

$$(\rho C_p)_{\mathrm{nf}}=(1-\varphi)(\rho C_p)_{\mathrm{f}}+\varphi(\rho C_p)_{\mathrm{s}} \tag{8}$$

$$\frac{k_{\mathrm{nf}}}{k_{\mathrm{f}}}=\frac{(k_{\mathrm{s}}-2k_{\mathrm{f}})-2\varphi(k_{\mathrm{f}}-k_{\mathrm{s}})}{(k_{\mathrm{s}}+2k_{\mathrm{f}})+\varphi(k_{\mathrm{f}}-k_{\mathrm{s}})} \tag{9}$$

where φ is the nanoparticle volume fraction, k_{nf} – the thermal conductivity of the nanofluid, k_{f} and k_{s} are the thermal conductivities of the fluid and of the solid fractions, respectively, $(\rho C_p)_{\mathrm{nf}}$ is the heat capacity of the nanofluid.

For present problem, Mahmood and Merkin introduce the similarity transformations [32]:

$$\psi = \sqrt{\frac{U_\infty \nu_f a^2}{\ell}} x f(\eta), \quad T - T_\infty = \Delta T \frac{x}{\ell} \theta(\eta), \quad \eta = \frac{r^2 - a^2}{2\nu_f \ell} \sqrt{\frac{U_\infty \nu_f \ell}{a^2}} \tag{10}$$

where ψ is the stream function defined in the usual form as $u = -(1/r)(\partial\psi/\partial r)$ and $v = -(1/r)(\partial\psi/\partial x)$ Substituting the transformations (10) into eqs. (2) and (3), we obtain a system of dimensionless non-linear ordinary differential equations:

$$\frac{1}{(1-\varphi)^{2.5}\left[1-\varphi+\varphi\left(\frac{\rho_s}{\rho_f}\right)\right]}[(1+2\gamma\eta)f''' + 2\gamma f''] + ff'' - f'^2 + \\ + \frac{(1-\varphi)+\varphi\left(\frac{\rho_s}{\rho_f}\right)\left(\frac{\beta_s}{\beta_f}\right)}{(1-\varphi)+\varphi\left(\frac{\rho_s}{\rho_f}\right)}\lambda\theta + 1 = 0 \tag{11}$$

$$\frac{1}{\Pr}\frac{\frac{k_{nf}}{k_f}}{\frac{1-\varphi+\varphi(\rho C_p)}{(\rho C_p)_f}}[(1+2\gamma\eta)\theta'' + 2\gamma\theta'] + \phi\theta' - f'\theta = 0 \tag{12}$$

subject to boundary conditions:

$$f(0) = 0, \quad f'(0) = 0, \quad f'(\infty) = 1 \tag{13}$$

$$\theta(0) = 1, \quad \theta(\infty) = 0 \tag{14}$$

where the primes denote differentiation with respect to η, f is the function related to the velocity field, and θ – the dimensionless temperature in the nanofluid, Pr – the Prandtl number, λ – the mixed convection parameter, and γ – the curvature parameter, which are defined as:

$$\lambda = \frac{\mathrm{Gr}}{\mathrm{Re}^2}, \quad \gamma = \sqrt{\frac{\nu_f \ell}{U_\infty a^2}} \tag{15}$$

where Gr is the Grashof number and Re – the Reynolds number. It should be noticed that $\lambda > 0$ corresponds to a heated cylinder (assisting flow), $\lambda < 0$ corresponds to a cooled cylinder (opposing flow), and $\lambda = 0$ corresponds to forced convection flow ($T_w = T_\infty$).

Series solution by means of HAM

The first step in the HAM is to find a set of base functions to express the sought solution of the problem under investigation. As mentioned by Liao [7], a solution may be expressed with different base functions, among which some converge to the exact solution of the problem faster than the others. Here, due to many boundary layer flows decay exponentially at infinity, we assume that $f(\eta)$ and $\theta(\eta)$ can be expressed by a set of functions:

$$\{\eta^k \exp(-n\eta) \mid k \geq 0, n \geq 0\} \tag{16}$$

in the form:

$$f(\eta) = a_{0,0} + \sum_{k=0}^{+\infty}\sum_{n=1}^{+\infty} a_{k,n}\eta^k \exp(-n\eta) \tag{17}$$

$$\theta(\eta) = \sum_{k=0}^{+\infty}\sum_{n=0}^{+\infty} b_{k,n}\eta^k \exp(-n\eta) \tag{18}$$

where $a_{k,n}$ and $b_{k,n}$ are coefficients. Thus, all approximations of $f(\eta)$ and $\theta(\eta)$ must obey the above expressions: this point is so important in the frame of the homotopy analysis method that it is regarded as a rule, called the *rule of solution expression* for $f(\eta)$ and $\theta(\eta)$. According to the boundary conditions (13) and (14) and the rule of solution expression defined by expressions (17) and (18), we choose:

$$f_0(\eta) = \eta - 1 + \exp(-\eta) \tag{19}$$

$$\theta_0(\eta) = \exp(-\eta) \tag{20}$$

as the initial approximations of $f(\eta)$ and $\theta(\eta)$. Besides, we select the auxiliary linear operators $\mathcal{L}_1[f]$ and $\mathcal{L}_2[\theta]$ as:

$$\mathcal{L}_1[f] = f''' - f' \tag{21}$$

$$\mathcal{L}_2[\theta] = \theta'' - \theta \tag{22}$$

satisfying the following properties:

$$\mathcal{L}_1[c_1 + c_2\exp(\eta) + c_3\exp(-\eta)] = 0 \tag{23}$$

$$\mathcal{L}_2[c_4\exp(\eta) + c_5\exp(-\eta)] = 0 \tag{24}$$

where c_i, $i = 1$ to 5 are constants. The auxiliary linear operator $\mathcal{L}$ is chosen in the following way. Here, we give a short introduction for the choice of the auxiliary linear operator $\mathcal{L}_1$ as an example. Due to eq. (11), and for the sake of simplicity, we choose a third-order linear operator:

$$\mathcal{L}[u] = u''' + b_1(\eta)u'' + b_2(\eta)u' + b_3(\eta)u \tag{25}$$

where $b_1(\eta)$, $b_2(\eta)$, and $b_3(\eta)$ are functions to be determined. Let

$$u = c_1 a_1(\eta) + c_2 a_2(\eta) + c_3(\eta) \tag{26}$$

denote the common solution of $\mathcal{L}[u] = 0$, where c_1, c_2, and c_3 are constants independent upon η. To obey the solution expression (19) and to satisfy the boundary conditions (13), we choose the elementary solutions:

$$a_1(\eta) = 1, \quad a_2(\eta) = \exp(\eta), \quad a_3(\eta) = \exp(-\eta) \tag{27}$$

Enforcing

$$\mathcal{L}[a_i(\eta)] = 0, \quad i = 1, 2, 3 \tag{28}$$

we have

$$b_1(\eta) = b_3(\eta) = 0, \quad b_2(\eta) = -1 \tag{29}$$

Therefore, we have the auxiliary linear operator:

$$\mathcal{L}[u] = u''' - u' \tag{30}$$

In general, the linear operators can be chosen on basis of two rules. Firstly, they must satisfy the solution expressions denoted by (17) and (18). The basic solutions of these linear operators should be only contained (at most) the four terms η, $\exp(\eta)$, $\exp(-\eta)$ or constant. Secondly, to decide the basic solutions of these linear operators, all of boundary conditions in (13)

and (14) must be used to determine integral constants. Note that we also have freedom to choose the linear operators as long as they satisfy above-mentioned rules. For details, the readers are referred to [7].

Based on eqs. (11) and (12), we are led to define the following non-linear operators as:

$$\mathcal{N}_1[\hat{f}(\eta;p),\hat{\theta}(\eta;p)]=\frac{1}{(1-\varphi)^{2.5}\left[1-\varphi+\varphi\left(\frac{\rho_s}{\rho_f}\right)\right]}\left[(1+2\gamma\eta)\frac{\partial^3\hat{f}(\eta;p)}{\partial\eta^3}+2\gamma\frac{\partial^2\hat{f}(\eta;p)}{\partial\eta^2}\right]+$$

$$+\frac{\partial\hat{f}(\eta;p)}{\partial\eta}\frac{\partial^2\hat{f}(\eta;p)}{\partial\eta^2}-\left(\frac{\partial\hat{f}(\eta;p)}{\partial\eta}\right)^2\frac{(1-\varphi)+\varphi\left(\frac{\rho_s}{\rho_f}\right)\left(\frac{\beta_s}{\beta_f}\right)}{(1-\varphi)+\varphi\left(\frac{\rho_s}{\rho_f}\right)}\lambda\hat{\theta}(\eta;p)+1 \tag{31}$$

$$\mathcal{N}_2[\hat{f}(\eta;p),\hat{\theta}(\eta;p)]=\frac{1}{\Pr}\frac{\frac{k_{nf}}{k_f}}{\left[\frac{1-\varphi+\varphi(\rho C_p)_s}{(\rho C_p)_f}\right]}\left[(1+2\gamma\eta)\frac{\partial^2\hat{\theta}(\eta;p)}{\partial\eta^2}+2\gamma\frac{\partial\hat{\theta}(\eta;p)}{\partial\eta}\right]+$$

$$+\hat{f}(\eta;p)\frac{\partial\hat{\theta}(\eta;p)}{\partial\eta}-\frac{\partial\hat{f}(\eta;p)}{\partial\eta}\theta(\eta;p) \tag{32}$$

where $p\in[0,1]$ is an embedding parameter and $\hat{f}(\eta;p)$ and $\hat{\theta}(\eta;p)$ are a kind of mapping function for $f(\eta)$ and $\theta(\eta)$, respectively. Using these operators, we can construct the zeroth-order deformation equations as:

$$(1-p)\mathcal{L}_1[\hat{f}(n;p)-f_0(\eta)]=p\hbar\mathcal{N}_1[\hat{f}(\eta;p),\hat{\theta}(\eta;p)] \tag{33}$$

$$(1-p)\mathcal{L}_2[\hat{f}(n;p)-\theta_0(\eta)]=p\hbar\mathcal{N}_2[\hat{f}(\eta;p),\hat{\theta}(\eta;p)] \tag{34}$$

where $\hbar$ is an auxiliary non-zero parameter. The boundary conditions for eqs. (33) and (34) are:

$$\hat{f}(0;p)=0,\quad \hat{f}'(0;p)=0,\quad \hat{f}'(\infty;p)=1 \tag{35}$$

$$\hat{\theta}(0;p)=1,\quad \hat{\theta}(\infty;p)=0 \tag{36}$$

Obviously, when $p=0$ and $p=1$ the above zeroth-order deformation equations have the following solutions:

$$\hat{f}(\eta;0)=f_0(\eta),\quad \hat{\theta}(\eta;0)=\theta_0(\eta) \tag{37}$$

$$\hat{f}(\eta;1)=f(\eta),\quad \hat{\theta}(\eta;1)=\hat{\theta}(\eta) \tag{38}$$

As p increases from 0 to 1, $\hat{f}(\eta;p)$ and $\hat{\theta}(\eta;p)$ vary from $f_0(\eta)$ and $\theta_0(\eta)$ to $f(\eta)$ and $\theta(h)$. By Taylor's theorem and eqs. (37) and (38) one obtains:

$$\hat{f}(\eta;p)=f_0(\eta)\sum_{m=1}^{+\infty}f_m(\eta)p^m \tag{39}$$

$$\hat{\theta}(\eta;p)=\theta_0(\eta)+\sum_{m=1}^{+\infty}\theta_m(\eta)p^m \tag{40}$$

where

$$f_m(\eta)=\frac{1}{m!}\frac{\partial^m\hat{f}(\eta;p)}{\partial p^m}\bigg|_{p=0},\quad \theta_m(\eta)=\frac{1}{m!}\frac{\partial^m\hat{\theta}(\eta;p)}{\partial p^m}\bigg|_{p=0} \tag{41}$$

As pointed by Liao [7], the convergence of the series (39) and (40) strongly depend upon auxiliary parameter $\hbar$. Assume that $\hbar$ is selected such that the series (39) and (40) are convergent at $p = 1$, then due to eqs. (37) and (38) we have:

$$f(\eta) = f_0(\eta) \sum_{m=1}^{+\infty} f_m(\eta) \tag{42}$$

$$\theta(\eta) = \theta_0(\eta) \sum_{m=1}^{+\infty} \theta_m(\eta) \tag{43}$$

For the m^{th}-order deformation equations, we differentiate eqs. (33) and (34) m times with respect to p, divide by $m!$ and then set $p = 0$. The resulting deformation equations at the m^{th}-order are:

$$\mathcal{L}_1[f_m(\eta) - \chi_m f_{m-1}(\eta)] = \hbar R_{1,m}(\eta) \tag{44}$$

$$\mathcal{L}_2[\theta_m(\eta) - \chi_m \theta_{m-1}(\eta)] = \hbar R_{2,m}(\eta) \tag{45}$$

with the following boundary conditions:

$$f_m(0) = 0, \quad f_m'(0) = 0, \quad f_m'(\infty) = 0 \tag{46}$$

$$\theta_m(0) = 0, \quad \theta_m(\infty) = 0 \tag{47}$$

where

$$R_{1,m}(\eta) = \frac{1}{(1-\varphi)^{2.5}\left[1-\varphi+\varphi\left(\frac{\rho_{\text{s}}}{\rho_{\text{f}}}\right)\right]}[(1+2\gamma\eta)f_{m-1}'''(\eta) + 2\gamma f_{m-1}''(\eta)] +$$

$$+\sum_{n=0}^{m-1}[f_n'(\eta)f_{m-1-n}''(\eta) - f_n'(\eta)f_{m-1-n}'(\eta)] + \frac{(1-\varphi)+\varphi\left(\frac{\rho_{\text{s}}}{\rho_{\text{f}}}\right)\left(\frac{\beta_{\text{s}}}{\beta_{\text{f}}}\right)}{(1-\varphi)+\left(\frac{\rho_{\text{s}}}{\rho_{\text{f}}}\right)}\lambda\theta_{m-1}(\eta) + (1-\chi_m) \tag{48}$$

$$R_{2,m}(\eta) = \frac{1}{\text{Pr}}\frac{\frac{k_{\text{nf}}}{k_{\text{f}}}}{\left[1-\varphi+\varphi\frac{(\rho C_p)_{\text{s}}}{(\rho C_p)_{\text{f}}}\right]}[(1+2\gamma\eta)\theta_{m-1}''(\eta) + 2\gamma\theta_{m-1}'(\eta)] +$$

$$+\sum_{n=0}^{m-1}[f_n(\eta)\theta_{m-1-n}'(\eta) - f_n'(\eta)f_{m-1-n}'(\eta)] \tag{49}$$

and

$$\chi_m = \begin{cases} 0, & m \le 1 \\ 1, & m > 1 \end{cases} \tag{50}$$

Let $f_m^*(\eta)$ and $\theta_m^*(\eta)$ denote the particular solutions of eqs. (48) and (49). From eqs. (23) and (24), their general solutions read:

$$f_m(\eta) = f_m^*(\eta) + c_1 + c_2\exp(\eta) + c_3\exp(-\eta) \tag{51}$$

$$\theta_m(\eta) = \theta_m^*(\eta) + c_4\exp(\eta) + c_5\exp(-\eta) \tag{52}$$

where the coefficients c_{i}, $i = 1$ to 5, are determined by the boundary conditions (46) and (47), *i. e.*

$$c_2 = c_4 = 0, \quad c_1 = -c_3 - f_m^*(0), \quad c_3 = \left.\frac{\partial f_m^*(\eta)}{\partial \eta}\right|_{\eta=0}, \quad c_5 = -\theta_m^*(0) \tag{53}$$

In this way, it is easy to solve the linear eqs. (44) and (45), one after the other in the order m = 1, 2, 3,..., especially by means of the symbolic computation software, such as Mathematica, Maple, and so on.

The similarity analysis of the steady axisymmetric mixed convective boundary layer flow of a nanofluid over a vertical circular cylinder results in a set of coupled non-linear ordinary differential equations for $f'(\eta)$ and $\theta(\eta)$ which are subject to the boundary conditions given by eqs. (13) and (14). These equations were solved analytically using the homotopy analysis method in the present study. The explicit analytic solutions given in eqs. (42) and (43) contain the auxiliary parameter $\hbar$ which give the convergence region and rate of approximation for the HAM solution. The reader is referred to [7] for the detailed discussion regarding the role of auxiliary parameters on the convergence region. Proper values for this auxiliary parameter can be found by plotting the so-called $\hbar$-curve.

Results and discussion

In the present study, three types of nanoparticles are considered, namely, alumina (Al_2O_3), titania (TiO_2), and copper (Cu). We have used data related to the thermophysical properties of the fluid and nanoparticles as listed in tab. 1 [33] to compute each case of the nanofluid. Following former studies, the value of the Prandtl number is taken as 6.2 (for water) and the volume fraction of nanoparticles is from 0 to 0.2 ($0 \le \varphi \le 0.2$) in which $\varphi = 0$ corresponds to the regular Newtonian fluid.

Table 1. Thermophysical properties of fluid and nanoparticles [33]

Thermophysical properties	Fluid phase (water)	Al_2O_3	TiO_2	Cu
C_p [Jkg^{-1}K^{-1}]	4179	765	686.2	385
ρ [kgm^{-3}]	997.1	3970	4250	8933
k [Wmk^{-1}]	0.613	40	8.9538	400
$\alpha \times 10^7$ [m^{2}s^{-1}]	1.47	131.7	30.7	1163.1

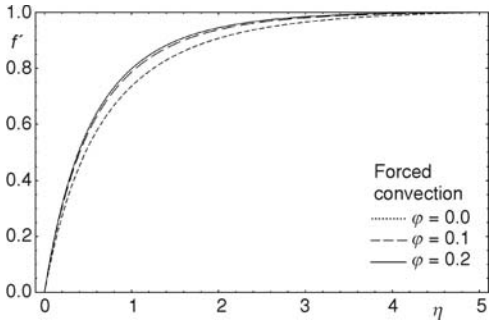

Figure 1. The influence of the different nanoparticle volume fractions on the velocity profile in the forced convection with copper-water nanofluid, when Pr = 6.2, γ = 1, and λ = 0

Figures 1 and 2 illustrate the influence of the different nanoparticle volume fractions on $f'(\eta)$ and $\theta(\eta)$ for forced convection flow ($\lambda = 0$) with copper-water nanofluid. From figs. 1 and 2, it is observed that the both velocity and temperature increase with the increase in the nanoparticle volume fraction parameter φ. For mixed convection flow (λ = 1) with copper-water nanofluid, the influence of the different nanoparticle volume fractions on the velocity and temperature profiles is shown in figs. 3 and 4. Figures 4 and 5 show the effect of the different nanoparticle volume fractions on the velocity and temperature profiles for the limit of free

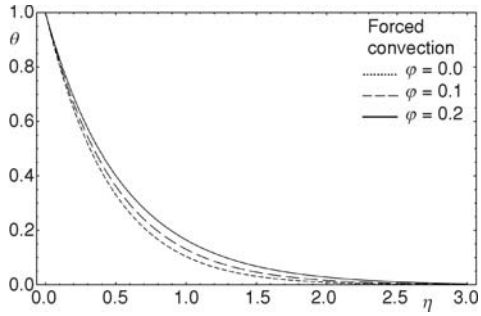

Figure 2. The influence of the different nanoparticle volume fractions on the temperature profile in the forced convection with copper-water nanofluid, when Pr = 6.2, $\gamma = 1$, and $\lambda = 0$

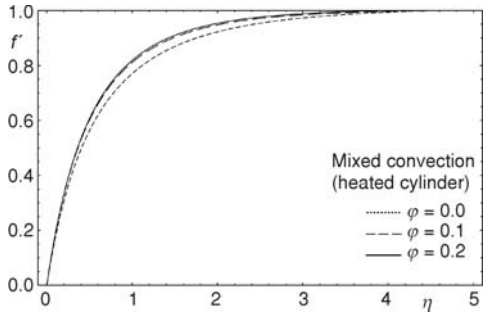

Figure 3. The influence of the different nanoparticle volume fractions on the velocity profile in the mixed convection with copper-water nanofluid, when Pr = 6.2, $\gamma = 1$, and $\lambda = 1$

convection (the large values of λ). Obviously, from figs. 3-6, we can see that the both velocity and temperature increase with the increase in the nanoparticle volume fraction parameter φ. An important point to note is that, for the limit of free convection, the velocity profile shows an overshoot near the wall (fig. 5) and this is in good agreement with the results reported by Mahmood and Merkin [32] and Grosan and Pop [34].

The influence of the different nanoparticles on $f'(\eta)$ and $\theta(\eta)$ is shown in figs. 7 and 8. Obviously, from fig. 7, copper-water and alumina-water nanofluids have the highest and lowest velocities components, respectively. Besides, fig. 8 demonstrates copper-water and alumina-water nanofluids have the lowest and highest temperature, respectively.

The two important physical quantities of present problem are the skin friction coefficients C_f and the local Nusselt number, which are defined as:

$$C_f = \frac{\tau_w}{\rho_f U_\infty^2}, \quad \mathrm{Nu} = \frac{\ell q_w}{k_f \Delta T} \tag{54}$$

In above equations, τ_w is the shear stress at the surface of the cylinder and q_w is the surface heat flux from the surface of the cylinder, which are given by:

$$\tau_w = \mu_{nf}\left(\frac{\partial u}{\partial r}\right)_{r=a}, \quad q_w = -k_f\left(\frac{\partial T}{\partial r}\right)_{r=a} \tag{55}$$

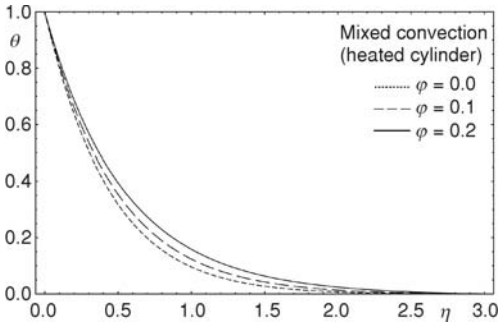

Figure 4. The influence of the different nanoparticle volume fractions on the temperature profile in the mixed convection with copper-water nanofluid, when Pr = 6.2, $\gamma = 1$, and $\lambda = 1$

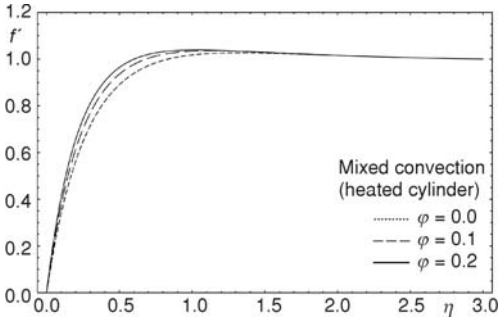

Figure 5. The influence of the different nanoparticle volume fractions on the velocity profile in the mixed convection with copper-water nanofluid, when Pr = 6.2, $\gamma = 1$, and $\lambda = 10$

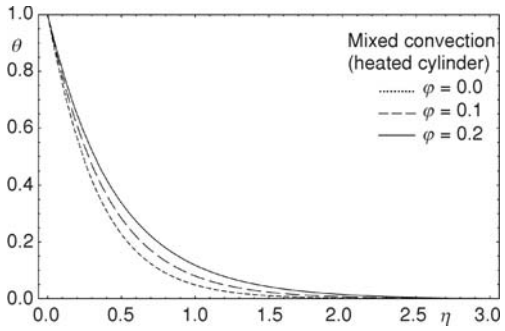

Figure 6. The influence of the different nanoparticle volume fractions on the temperature profile in the mixed convection with copper-water nanofluid, when Pr = 6.2, $\gamma = 1$, and $\lambda = 10$

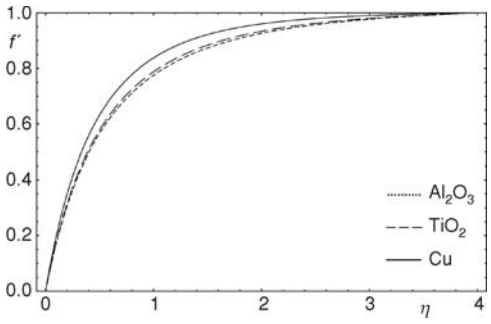

Figure 7. The influence of the different nanoparticles (alumina, titania and copper) on the velocity profile in the mixed convection, when Pr = 6.2, $\gamma = 1$, and $\lambda = 2$

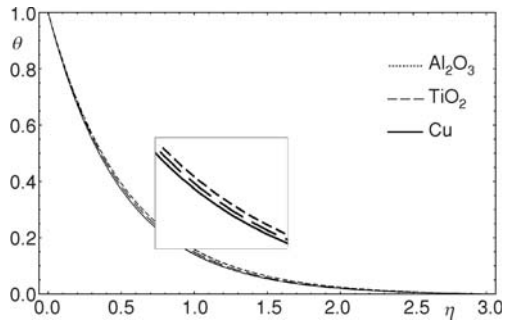

Figure 8. The influence of the different nanoparticles (alumina, titania, and copper) on the temperature profile in the mixed convection, when Pr = 6.2, $\gamma = 1$, and $\lambda = 2$

Using eq. (10), (54), and (55), we obtain:

$$\sqrt{\mathrm{Re}}C_{\mathrm{f}} = \frac{\bar{x}}{(1-\varphi)^{2.5}} f''(0)$$

$$\frac{1}{\sqrt{\mathrm{Re}}}\mathrm{Nu} = -\frac{k_{\mathrm{nf}}}{k_{\mathrm{f}}}\bar{x}\theta'(0) \qquad (56)$$

where $\bar{x} = x/\ell$. It is worth noting that the present study reduces to that of Mahmood and Merkin [8] for a viscous fluid when $\varphi = 0$ (regular fluid).

Table 2 displays the influence of the different nanoparticle volume fractions on the skin friction coefficients and the local Nusselt number for the different nanoparticles. To verify accuracy of HAM solution, we have inserted numerical results for nanoparticles reported by Grosan and Pop [34]. We can see a very good agreement between the purely analytic results of the HAM and numerical results. From tab. 2, for all three nonoparticles, it is observed that the skin friction coefficient and the local Nusselt number increase with increasing in the nanoparticle volume fraction. An important point to note is that the Cu nanoparticles has the highest skin friction coefficient. Moreover, it is noted that the highest heat transfer rate is also obtained for the Cu nanoparticles. This is because Cu has the highest value of thermal conductivity compared to TiO_2 and Al_2O_3. The reduced value of thermal diffusivity leads to higher temperature gradients and, therefore, higher enhancements in heat transfer. The Cu nanoparticles have high values of thermal diffusivity and, therefore, this reduces temperature gradients which will affect the performance of Cu nanoparticles. In spite of this point, when the nanoparticle volume fraction is increased from 0 to 0.2, we can see that the highest enhancement in the Nusselt number is for the Cu nanoparticles (see tab. 2).

Final remarks

In this article, the homotopy analysis method is employed to study the steady axisymmetric mixed convective boundary layer flow of a nanofluid over a vertical circular cyl-

Table 2. The influence of the different nanoparticle volume fractions on the skin friction coefficients and the Nusselt number for the different nanoparticles, and comparison with Grosan and Pop's numerical solution, when Pr = 6.2 and $\gamma = 1$

Nanoparticle	λ	φ	$(1/\bar{x})\sqrt{\mathrm{Re}}C_f$		$(1/\bar{x})\mathrm{Re}^{-1/2}\mathrm{Nu}$	
			Present study	Grosan and Pop [34]	Present study	Grosan and Pop [34]
Al_2O_3	0	0.0	1.70764		2.15177	
		0.1	2.23358		2.83887	
		0.2	2.90387		3.09029	
	1	0.0	1.99210		2.21366	
		0.1	2.52204		2.65785	
		0.2	3.20388		3.14234	
	5	0.0	3.02007		2.40937	
		0.1	3.59353		2.84704	
		0.2	4.32866		3.32189	
TiO_2	0	0.0	1.70746		2.15177	
		0.1	2.24884		2.53340	
		0.2	2.93952		2.93368	
	1	0.0	1.99210		2.21366	
		0.1	2.52762		2.58652	
		0.2	3.21555		2.97913	
	5	0.0	3.02007		2.40937	
		0.1	3.55914		2.76413	
		0.2	4.25507		3.13753	
Cu	0	0.0	1.70764	1.70762	2.15177	2.15173
		0.1	2.51216	2.51213	2.69664	2.69667
		0.2	3.46826	3.46829	3.26935	3.26938
	1	0.0	1.99210	1.99215	2.21366	2.21362
		0.1	2.79276	2.79271	2.74838	2.74831
		0.2	3.75691	3.75699	3.31539	3.31533
	5	0.0	3.02007	3.02004	2.40937	2.40935
		0.1	3.83616	3.83609	2.92289	2.92285
		0.2	4.84849	4.84841	3.47660	3.47668

inder. Here, three different types of nanoparticles are considered, namely alumina, titania, and copper with water as the base fluid. Finally, from the presented analysis, the following observations are noted.

- For the forced and mixed convection flows of copper-water nanofluid, the velocity and temperatuer increase with the increase in the nanoparticle volume fraction.
- Comparing between three nanoparticles, copper-water and alumina-water nanofluids have the highest and lowest velocities components, respectively.
- For all three nonoparticles, it is observed that the skin friction coefficient and the local Nusselt number increase with the increase in the nanoparticle volume fraction.
- The skin friction coefficient and the heat transfer rate at the surface are highest for copper-water nanofluid compared to the alumina-water and titania-water nanofluids.

- The type of nanofluid is a key factor for heat transfer enhancement. The highest values are obtained when using nanoparticles.

Nomenclature

a – radius of cylinder, [m]
C_f – skin friction coefficient, [–]
C_p – specific heat at constant pressure, [$Jkg^{-1}K^{-1}$]
$f(h)$ – similarity function, [–]
Gr – Grashof number, [$= g\beta_f \Delta T \ell^3/\nu_f^2$]
g – gravity acceleration, [ms^{-2}]
$\hbar$ – auxiliary convergence-control parameter, [–]
k – thermal conductivity coefficient, [$Wm^{-1}K^{-1}$]
ℓ – characteristic length of the cylinder, [m]
$\mathcal{L}$ – linear operator
$\mathcal{N}$ – non-linear operator
Pr – Prandtl number, [$= \nu_f/\alpha_f$]
P – embedding parameter, [–]
q_w – heat flux from the surface of the cylinder, [Wm^{-2}]
Re – Reynolds number, [$= U_\infty \ell/\nu_f$]
r – radial co-ordinate, [m]
T – temperature of the nanofluid, [K]
$T_w(x)$ – wall temperature, [K]
T_∞ – ambient temperature, [K]
ΔT – characteristic temperature, [K]
$U(x)$ – velocity of the external flow, [ms^{-1}]
U_∞ – characteristic velocity, [ms^{-1}]
u – velocity component along, [ms^{-1}]
w – velocity component along, [ms^{-1}]
x – axial co-ordinate, [m]
$\bar{x}$ – dimensionless axial co-ordinate, [–]

Greek symbols

α – thermal diffusivity, [$m^2K^{-1}s^{-1}$]
β – thermal expansion coefficient, [–]
γ – curvature parameter, [–]
η – similarity variable, [–]
$\theta(\eta)$ – dimensionless temperature, [–]
λ – mixed convection parameter, [–]
μ – dynamic viscosity, [$kgm^{-1}s^{-1}$]
ν – kinematic viscosity, [m^2s^{-1}]
ρ – density, [kgm^{-3}]
τ_w – wall skin friction, [$kgm^{-1}s^{-1}$]
φ – nanoparticle volume fraction, [–]
ψ – streamline function, [–]

Subscripts

f fluid
nf nanofluid
s solid

References

[1] Gebhart, B., *et al*., *Buoyancy-Induced Flows and Transport*, Hemisphere, New York, USA, 1988
[2] Martynenko, O. G., Khramtsov, P. P., *Free-Convective Heat Transfer*, Springer, Berlin, 2005
[3] Chen, T. S., Mucoglu, A., Buoyancy Effects on Forced Convection along a Vertical Cylinder, *J. Heat Transfer, 97* (1975), 2, pp. 198-203
[4] Mahmood, T., Merkin, J. H., Mixed Convection on a Vertical Circular Cylinder, *J. Appl. Math. Phys. (ZAMP), 39* (1988), 2, pp. 186-203
[5] Ishak, A., *et al*., The Effects of Transpiration on the Boundary Layer Flow and Heat Transfer over a Vertical Slender Cylinder, *Int. J. Non-Linear Mech., 42* (2007), 8, pp. 1010-1017
[6] Liao, S. J., The Proposed Homotopy Analysis Technique for the Solution of Non-Linear Problems, Ph. D. thesis, Shanghai Jiao Tong University, China, 1992
[7] Liao, S. J., *Beyond Perturbation: Introduction to the Homotopy Analysis Method*, Chapman and Hall/CRC Press, Boca Raton, Fla., USA, 2003
[8] Liao, S. J., A Kind of Approximate Solution Technique which Does Not Depend upon Small Parameters (II): An Application in Fluid Mechanics, *Int. J. of Non-Linear Mech., 32* (1997), 5, pp. 815-822
[9] Liao, S. J., An Explicit, Totally Analytic Approximation of Blasius Viscous Flow Problems, *Int. J. Nonlinear Mech., 34* (1999), 4, pp. 759-778
[10] Liao, S. J., A Uniformly Valid Analytic Solution of 2-D Viscous Flow Past a Semi-Infinite Flat Plate, *J. Fluid Mech., 385* (1999), Apr., pp. 101-128
[11] Liao, S. J., On the Homotopy Analysis Method for Nonlinear Problems, *Appl. Math. Comput., 147* (2004), 1, pp. 499-513
[12] Liao, S. J., Tan, Y., A General Approach to Obtain Series Solutions of Nonlinear Differential Equations, *Studies in Applied Mathematics, 119* (2007), 4, pp. 297-355

[13] Liao, S. J., Beyond Perturbation: a Review on the Basic Ideas of the Homotopy Analysis Method and its Applications (in Chinese), *Advanced Mechanics, 38* (2008), pp. 1-34
[14] Abbasbandy, S., The Application of Homotopy Analysis Method to Nonlinear Equations Arising in Heat Transfer, *Phys. Lett., A 360* (2006), 1, pp. 109-113
[15] Abbasbandy, S., Approximate Solution for the Non-Linear Model of Diffusion and Reaction in Porous Catalysts by Means of the Homotopy Analysis Method, *Chemical. Eng. J., 136* (2008), 2-3, pp. 144-150
[16] Allan, F. M., Syam, M. I., On the Analytic Solution of Non-Homogeneous Blasius Problem, *J. Comput. Appl. Math., 182* (2005), 2, pp. 362-371
[17] Hayat, T., Javed, T., On Analytic Solution for Generalized Three-Dimensional MHD Flow over a Porous Stretching Sheet, *Phys. Lett., A 370* (2007), 5-6, pp. 243-250
[18] Sajid, M., *et al*., Wire Coating Analysis Using MHD Oldroyd 8-Constant Fluid, Int. J. Eng. Sci. 45 (2007), 2, pp. 381-392
[19] Dinarvand, S., A Reliable Treatment of the Homotopy Analysis Method for Viscous Flow over a Non-Linearly Stretching Sheet in Presence of a Chemical Reaction and under Influence of a Magnetic Field, *Cent. Eur. J. Phys., 7* (2009), 1, pp. 114-122
[20] Dinarvand, S., On Explicit, Purely Analytic Solutions of Off-Centered Stagnation Flow Towards a Rotating Disc by Means of HAM, *Nonlinear Anal. Real World Appl., 11* (2010), 6, pp. 3389-3398
[21] Cheng, J., *et al*., Series Solutions of Nano Boundary Layer Flows by Means of the Homotopy Analysis Method, *J. Math. Anal. Appl., 343* (2008), 1, pp. 233-245
[22] Dinarvand, S., The Laminar Free-Convection Boundary-Layer Flow about a Heated and Rotating Down-Pointing Vertical Cone in the Presence of a Transverse Magnetic Field, *Int. J. Numer. Meth. Fluids*, *67* (2011), 12, pp. 2141-2156
[23] Dinarvand, S., Rashidi, M. M., A Reliable Treatment of Homotopy Analysis Method for Two-Dimensional Viscous Flow in a Rectangular Domain Bounded by Two Moving Porous Walls, *Nonlinear Anal. Real World Appl., 11* (2010), 3, pp. 1502-1512
[24] Dinarvand, S., *et al.*, Series Solutions for Unsteady Laminar MHD Flow Near Forward Stagnation Point of an Impulsively Rotating and Translating Sphere in Presence of Buoyancy Forces, *Nonlinear Anal. Real World Appl., 11* (2010), 2, pp. 1159-1169
[25] Kousar, N., Liao, S. J., Series Solution of Non-Similarity Boundary-Layer Flows over a Porous Wedge, *Transport in Porous Media, 83* (2010), 2, pp. 397- 412
[26] Khan, M., *et al*., Steady Flow and Heat Transfer of a Sisko Fluid in Annular Pipe, *Int. J. Heat Mass Transfer, 53* (2010), 708, pp. 1290-1397
[27] Khan, M., *et al*., Heat Transfer Analysis of the Steady Flow of an Oldroyd 8-Constant Fluid Due to a Suddenly Moved Plate, *Commun. Nonlinear Sci. Numer. Simulat., 16* (2011), 3, pp. 1347-1355
[28] Tiwari, R. K., Das, M. K., Heat Transfer Augmentation in a Two-Sided Lid-Driven Differentially Heated Square Cavity Utilizing Nanofluids, *Int. J. Heat Mass Transfer, 50* (2007), 9-10, pp. 2002-2018
[29] Ellahi, R., Series Solutions for Magnetohydrodynamic Flow of Non-Newtonian Nanofluid and Heat Transfer in Coaxial Porous Cylinder with Slip Conditions, *J. Nanoengineering and Nanosystems, 225* (2011), 3, pp. 123-132
[30] Ellahi, R., *et al*., Series Solutions of Non-Newtonian Nanofluids with Reynolds' Model and Vogel's Model by Means of the Homotopy Analysis Method, *Math. Compu. Modelling, 55* (2012), 7-8, pp. 1876-189
[31] Ellahi, R., The Effects of MHD and Temperature Dependent Viscosity on the Flow of Non-Newtonian Nanofluid in a Pipe: Analytical Solutions, *Appl. Math. Modeling, 55* (2012), 23-24, pp. 6384-6390
[32] Mahmood, T., Merkin, J. H., Similarity Solutions in Axisymmetric Mixed Convection Boundary-Layer Flow, *J. Eng. Math., 22* (1988), 1, pp. 73-92
[33] Oztop, H. F., Abu-Nada, E., Numerical Study of Natural Convection in Partially Heated Rectangular Enclosures Filled with Nanofluids, *Int. J. Heat Fluid Flow, 29* (2008), 5, pp. 1326-1336
[34] Grosan, T., Pop, I., Axisymmetric Mixed Convection Boundary Layer Flow Past a Vertical Cylinder in a Nanofluid, *Int. J. Heat Mass Transfer, 54* (2011), 15-16, pp. 3139-3145

Paper submitted: February 25, 2012
Paper revised: September 2, 2012
Paper accepted: September 12, 2012